Vegan chocolate formulation using plant-based fat mixtures: a study on crystallization phenomena

*Cecilia Fiore[1], Luca Violato[1], Irene Giovando[1], Tom Rutherford[3], Stephanie Marty Terrade[4], Francesca Giuffrida[4], Cynthia Marmet[4], Elena Simone[1,2]**

[1] Department of Applied Science and Technology (DISAT), Politecnico di Torino, Torino, Italy

[2] School of Food Science and Nutrition, Food Colloids and Bioprocessing Group, University of Leeds, Leeds, United Kingdom

[3] Nestlé Product Technology Centre Confectionery, Haxby Road, York, YO31 8TA, United Kingdom

[4] Nestlé Research, Vers-chez-les-Blanc, Lausanne 26, 1000, Switzerland

Corresponding author: *Professor Elena Simone, tel. +39 0110904652, email: elena.simone@polito.it

KEYWORDS: Milk fat; chocolate; crystallization; X-ray scattering; triacylglycerides (TAGs)

ABSTRACT

Due to increasing global demand for chocolate products and changes in consumer preferences chocolate manufacturers have recently started to explore novel solutions to reformulate chocolate. Milk fat equivalents and replacers (MFE, MFR) are mixtures of triglycerides from different plant-based sources that resemble milk fat in its physical properties; they are potential ingredients for vegan milk chocolate formulations. Here, we applied synchrotron X-ray scattering, polarized light

microscopy and differential scanning calorimetry, to investigate the crystallization behavior of four selected commercial MFEs (MF1, 2, 3, 4), on their own and mixed with cocoa butter (CB). Chemical characterization revealed significant differences among samples, and with both milk fat (MF) and CB. Due to chemical similarity with CB, mixtures of samples MF2 and MF3 with CB, performed similarly to pure CB in terms of number, type and morphology of polymorphs crystallized. Despite significant differences in chemical composition, MF4 presented similar crystallization behavior, texture and solid fat content of MF. This is due to the high percentage of unsaturated fatty acids and the wide variety of triacylglycerides that characterize MF4. POP rich MF1 presented a specific polymorphic and thermal behavior, with the unstable β' form persisting for longer times than all other samples.

INTRODUCTION

Chocolate is a complex food product widely consumed throughout the world. It can be described as a fat-continuous matrix, where triacylglycerides (TAGs) are the key constituents, within which some non-fat solid particles, generally sugar and cocoa powder are dispersed.[1] This fat phase, which defines many of the quality attributes of the final product, is mainly composed of cocoa butter (CB), a natural fat obtained from the seeds of the cocoa tree (*Theobroma cacao*).[1,2] In the last years the consumption of chocolate increased and consequently the demand for cocoa butter raised, resulting in a further increase in the cost of chocolate production.[2] In fact, from an economical perspective, cocoa butter is expensive compared to other edible oils and fats, due to its specific organoleptic features and considering the limited number of countries in which cocoa *Theobroma cacao* is cultivated.

Hence, significant effort has been made to find ways to replace CB in confectionary products to make chocolate production more sustainable from both an economical and environmental prespective.[2-5] One of the possible strategies is the blending of different plant-based fats to create cocoa butter

alternatives (CBAs), that can partially or even fully replace CB in chocolate recipes, still offering satisfactory functional properties such as melting point and texture.[2,6–8]

A good quality chocolate must have a shiny surface, a crunchy texture that is pleasant in the mouth and a good resistance to heat and blooming.[5,9–11] All these characteristics are influenced by the crystal structure of cocoa butter.[12,13] This plant-based fat is a complex mixture of TAGs and its crystallization behaviour can vary accordingly to its variable composition.[14] In fact, depending on the origin of the CB sample, the fatty acid and TAGs composition may slightly change.[15] However, usually CB is largely composed of palmitic acid (16:0), stearic acid (18:0), oleic acid (18:1), and, in lower quantity, of linoleic acid (18:2), and arachidic acid (20:0). This fatty acid composition generally results in three main triglycerides: 1(3)-palmitoyl-2-oleoyl-3(1)-stearoyl glycerol (POS), 1,3-dipalmitoyl-2-oleoyl glycerol (POP), and 1,3-distearoyl-2-oleoyl glycerol (SOS).[16,17] CB can form six different polymorphs named Form I to Form VI from the least to the most stable; these are characterised by different subcell geometries (2L or 3L), different unit cells (hexagonal α, orthorhombic β' or monoclinic β) and, hence different physical properties.[1,9,18] Only form V has the desired organoleptic properties for chocolate; hence, a good control over the crystallization process is essential for the production of a good quality chocolate.[11]

In dark or plain chocolate CB is usually the only fat present; whereas, milk fat (MF) can be added to obtain milk chocolate products with different taste and texture properties.[19–23]

Despite milk fat advantages are undoubted, and its usage consolidated, there are some important drawbacks related to the use of this fat. Particularly, it is not consumed by some categories of costumers, such as vegans or lactose intolerant. In addition, there are well known sustainability issues related to the dairy industry. For these reasons, the use of plant-based mixtures of triacylglycerides (TAGs) as MF replacers can be a possible solution to some of the aforementioned concerns; and the study of the crystallization behaviour of these MF replacers becomes of primary importance to enable their use in chocolate products. Plant-based TAGs mixtures are commonly applied as cocoa butter

equivalents (CBEs) and substitutes (CBS)[2,6,24,25] and when they are blended in different proportions with CB, their specific TAGs composition can influence the crystallization behaviour of chocolate and affect the functional properties of the final product (e.g., thermal, mechanical, mouthfeel).[8,14] Milk fat is one of the most complex fats in terms of composition, which varies widely depending on the feeding type and genetic differences of the species from which it is obtained[26]. It contains a variety of different fatty acids with a wide range of carbon chain lengths. One of the peculiar features of milk fat is the presence of a non-negligible amount of short-chain fatty acids (4:0 and 6:0). These are usually located on the sn-3 carbon of the TAG molecule. Both the amount and location of these shorter-chain fatty acids in the TAG molecules affect milk fat properties, such as melting point and flavour.[28] The most prevalent TAGs found in milk fat[26] are reported in **Table 1,** with their respective concentration (mol%).

In this work the crystallization behaviour of four plant-based TAGs mixtures commercialized as milk fat replacers (named MF1, MF2, MF3, MF4, MF*n*) was studied and compared to that of commercial anhydrous milk fat. Pure MFn and their mixtures with CB in ratios typical of milk chocolate were also characterized.

A combination of synchrotron X-ray scattering, differential scanning calorimetry (DSC), and polarized light microscopy were used to analyze the crystallization behavior of the MF*n* and their blends with CB. Samples were characterized also in terms of their TAGs and fatty acids composition via chromatographic techniques. These information were found to be essential to correctly interpret the structural information provided by X-ray scattering and obtaining a molecular level understanding of the crystallization behavior of such complex TAGs mixtures. This is crucial not only for creating innovative chocolate recipes incorporating CBEs and MF substitutes but also for understanding the crystallization patterns in other similar blends of TAGs, potentially usable in food, cosmetic, or pharmaceutical contexts.

MATERIALS AND METHODS

Materials: Samples of cocoa butter (CB), anhydrous milk fat (MF) and milk fat replacers (MFn; n=1,2,3,4) were provided by the Nestlè Product Technology Centre Confectionery in York (UK). CB is a cocoa butter sample of Ghanian origin, and MF is a milk fat sample derived from cow milk. MFn are TAGs plant-based mixtures as described in the introduction. MF1 is based on fractionated palm and shea oil while MF3 is based on exotic oils. MF2 is a fractionated, non-hydrogenated, refined vegetable fat of non-lauric origin. MF4 is a blend of fractionated and non-hydrogenated vegetable oils. All samples present different solid fat contents, as shown in **Table 2**, which are compatible with cocoa butter: MF*n* (*n*=1,2,3,4) samples were analysed and studied in the meaning of their possible use as MF replacers in a novel formulation of a vegan, lactose-free and more sustainable chocolate product. Their blends in a 20% proportion of MF*n* in CB were also analysed in comparison to a blend of 20% of MF in CB.

Preparation of cocoa butter, milk fat and milk fat replacers mixtures: 5 g of each sample were melted in a preheated oven at 70° C and kept for 1h to ensure the complete melt. Mixtures with 20% in mass of MF and MF*n* in CB (1 g of MF/MF*n* in 4g of CB) were prepared by weighing on a scale the required mass of each melted sample using a pipette and placed in 10 ml glass vials. The blends were then heated up again at 70° C and kept for another hour in the oven for a better mixing of the melted constituents.

Chemical characterization**:** CB, MF and MF*n* were characterized in terms of fatty acids (FA) and triacylglycerides composition by gas chromatography. An Accela 1250 liquid chromatograph (Thermo Fisher Scientific, Bremen, Germany) equipped with a Agilent Poroshell 120 EC-C18 (2.7 µm particle size, 2.1 × 250 mm) was used for separation of analytes; while an LTQ-Orbitrap XL hybrid mass spectrometer (Thermo Fisher Scientific, Bremen, Germany) was used for the identification of the TAGs and FAs that characterized each sample. The detailed experimental procedure is described elsewhere [29]. The TAGs composition of milk fat was evaluated according to the Zeb and Murkovich procedure[30] in a Shimadzu LCMS 2020 (Japan) with a separation column

Phenomenex Luna 3u C18(2) 100A LC Column 150 x 3.0 mm. The detailed procedure can be found in our previous work.[26] Measurements were performed in triplicates and the collected data were processed in the LabSolutions software (version 5.97) to obtain chromatograms and mass spectra. Further chromatograms peak fittings, integration and plotting were carried out using OriginPro 2019b. Prior to fitting, the solvent contribution was removed.

Differential Scanning Calorimetry (DSC): The DSC curves were obtained using a Mettler Toledo DSC 1 (Mettler Toledo, USA). Approximately 3mg of each sample were weighed and sealed in an aluminum pan, while an empty aluminum pan was used as a reference**.** Each sample was heated up to 70°C with a rate of 10°C/min, cooled to -10°C at -5°C/min, then re-heated to 70°C at 2°C/min and finally cooled to -10°C at -2°C/min. DSC traces are reported in **Supporting information, Section 4.**

Polarized light microscopy (PLM): Samples were heated in an oven at 50°C until fully molten. Approximately one drop of each sample was transferred on a glass slide using a plastic pipette and then covered with a cover glass. The glass slide was then placed onto a Linkam PE120 hot stage, connected to a water circulation pump (Linkam Scientific Instruments, UK). The hot plate was positioned on a Zeiss Axiolab 5 microscope (Zeiss, Germany) with a polarized light lens. The temperature was then varied with a T96 Peltier LinkPad controller. Each sample was heated up to 70°C at 10°C/min, then cooled down to 5 °C at -2°C/min, heated again to 70° C at 0.5°/min, and finally cooled to 5°C at -0.5°C/min. Videos of the crystallization and melting of the samples were recorded with an iPhone 13 camera set-up (Apple, USA), using the 40X magnification lens of the microscope. In **Figure 1.** is reported a graphical example of the image processing methodology applied. Videos and images were then processed using Matlab_R2023a, by extracting a frame every 30 s. For each frame the background was removed, then the truecolor image was converted into a grayscale and then into a binary one, composed of just black and white pixels, the latter representing the crystals. The number of white pixels in a specific image was then plotted as a function of time.

Powder X-ray Diffraction (PXRD): PXRD patterns for CB and MF were recorded with an Empyrean diffractometer (Malvern Panalytical, U.K). Diffraction patterns in the wide-angle region (2 θ range of 4-40°) were obtained using a CuK $_{\alpha}$ radiation with a wavelength (λ) of 1.54 Å. The instrument operated with an intensity of 40 mA and a voltage of 40 kV. The solid samples were grinded in an agate mortar and pestle before placing them onto a sample holder. The sample with a lower solid fat content at room temperature were directly pressed into the sample holder without grinding. The wide angles were converted to d-spacing values using Bragg's Law ($d = \frac{1}{2 \sin q}$) resulting in a range of 2.25-22 Å.

Synchrotron small angle X-ray scattering: SAXS measurements were performed at the SAXS beamline at the Elettra Sincrotrone facility in Trieste (Italy) and at the I22 beamline of Diamond Light Source (Didcot, UK). The energy of the beam used were 10 and 18keV respectively. At Elettra he SAXS patterns, in the range of q of 0.04-0.72 $Å^{-1}$ were recorded by a Pilatus3 1M detector (Dectris Ltd.,Switzerland). At Diamond SAXS 2D diffraction patterns were recorded on a Pilatus 2M detector (Dectris Ltd., Switzerland). For WAXS a Pilatus P3-2M-DLS-L (silicon hybrid pixel detector, Dectris Ltd., Switzerland). For both synchrotron setups, quartz capillaries were filled with the melted samples and placed at room temperature for 20 days before the experiments. The experiment temperature was varied using a Peltier element and temperature profiles used are reported in **Table 3**. The exposure times were 1s for beamline I22 and 20s for Elettra SAXS beamline. The data obtained from SAXS measurements were analyzed using Origin2018 (Originlab). In order to resolve overlapping peaks, small portions of data were analyzed individually, performing baseline correction if necessary and applying fitting routines with Gaussian or Voigt functions. Thus, the q values of the peaks at different diffraction order were obtained and used to determine the number and d-spacings of the different polymorphs present in the sample. The d-spacing is related to the q values through the following equation:

$$d = \frac{2\pi}{q} \quad (1)$$

In order to distinguish the lamellar phases present in each sample from the SAXS data, the values of q of every peak were plotted as a function of their diffraction order. The q values related to a specific lamellar phase lie on a straight line with slope equal to the characteristic d-spacing of the phase. If more than one phase is present, different straight lines can be identified with the q-values estimated.

RESULTS AND DISCUSSION

Chemical composition of MF, CB and MF replacers. The MF sample has a complex composition, with a wide variety of fatty acids present, which lead to a complex TAGs profile.[26] This is very different from the general composition of CB, which is usually mainly composed of POS, POP and SOS triglycerides. In the MF sample used in this work the TAG in the highest concentration is BuPO (7.2%), followed by BuMP (5.1%), BuPS (4.9%) and BuMO (4.4%). The complete TAGs composition of MF is reported in **Supporting Information, Section 1, Table 1**. The simplified TAGs composition of CB, MF and the MF*n* is instead shown in **Tables 4** and **5** and **Figure 2.**

Referring to **Table 4**, MF1 has the higher amount of POP followed by MF2 and CB, while MF3 and MF4 present a very low quantity of POP (<1 and 1.9 respectively), similarly to MF. MF3 possess a larger quantity of SOS and MF2 comes right after, still maintaining a more equilibrated proportion of POP and SOS. In MF3 the high amount of OOS and OOO is characterizing the unique profile of this TAGs mixture. MF4 has higher variety in terms of TAGs compared to the other samples; in fact, the respective amount of POP, POS and SOS is much lower (<6 %) and their sum does not exceed the 12% of the total.

In MF4, OOO and OOS are the major components, followed by SSO. All the MF*n* samples have a higher percentage of di-unsaturated TAGs compared to CB and MF, and among them MF3 has the largest amount, with a 33.1% of the total mixture. MF4 follows with 31.1% of di-unsaturated and it

also has the highest quantity of tri-unsaturated TAGs (18.8%). In comparison to CB, all four MFn also possess a higher percentage of tri-saturated TAGs, with the maximum of MF4 (3.9% of its total composition) compared to CB that has less than 1%. Considering our MF sample, that has 7.3% of tri-saturated TAGs, all MF*n* and CB have a smaller amount. The relative fatty acids (FA) composition is also crucial. Analysing the mixture in terms of distribution of saturated and unsaturated FA together with the average chain length allows to get a better understanding of the melting profile and crystallization behaviour of the samples. In fact, the melting point generally increases with chain length and decreases with unsaturation. TAGs with long and/or saturated chains are high melting, whereas those with polyunsaturated and/or shorter or asymmetric chains are lower melting. The FA composition is summarized in **Table 5,** which also reports the average chain length for each MF*n*, CB and MF. It is worth noticing the high amount of saturated FA in MF, which results also in high percentage of tri-saturated TAGs, and the significantly shorter average FA chain of MF compared to the rest of the samples. In fact, the presence of short FA (down to 4 C atoms) is responsible for the relatively low melting point and SFC of MF, despite the abundance of saturated FA.

Polymorph identification with PXRD and SAXS/WAXS measurements. The polymorphic forms present in the MFn solid samples at room temperature (20°C) were investigated both with small and wide angle X-ray scattering/diffraction. Dynamic crystallization experiments were also performed using synchrotron SAXS.[30]

The PXRD diffractogram of CB, shown in **Figure 3.(a)**, was indicative of the presence of the β(V) polymorph.[32] However, the SAXS data (**Figure 3.(b)**), (20°C) showed the presence of two immiscible β phases, in accordance to what observed by Simone et al.:[31] the β(V) (d=63.9 Å) and a higher melting β-2L (d=44 Å). SAXS patterns of CB collected during cooling, holding, and heating profiles are reported in **Supporting information, Section 2.1, Figure 1 (a-d)** and discussed by Simone et al.[31]

The PXRD diffractogram of MF at equilibrium conditions did not possess a clear baseline due to low solid fat content of MF at room temperature. In **Figure 4.(a)**,the peaks at q=1.427 $Å^{-1}$ (d=4.5 Å) and 1=1.636 $Å^{-1}$ were representative of a β' polymorph, whereas the weak peak at q=1.475 $Å^{-1}$ (d=4.3 Å) suggested the presence of traces of an α form.[35] These observations agreed with the SAXS pattern of **Figure 4.(b)** where two phases are noticeable, associated to a sharp peak at q=0.152 $Å^{-1}$ and a shoulder at lower values of q. The higher peak corresponding to a long spacing of 41.4 Å was consistent with the d-spacing value reported in the literature for the β'-2L polymorph for milk fat.[26] The weaker peak was likely associated to the α-2L (d=45.6 Å) polymorph.[36] The co-existence of these two phases was more evident at higher ranges of q, where the Bragg peaks did not overlap (e.g., the third order peaks of the α and β' phases at q= 0.41 $Å^{-1}$ and q=0.454 $Å^{-1}$). The presence of the α phase was also suggested by the peak at q=0.55 $Å^{-1}$, representing the fourth order of diffraction.

The crystallization and melting behavior was also studied and the results were in accordance with what previously reported by Pratama et al.[26]. All SAXS patterns collected during cooling, holding, and heating profiles are reported in **Supporting information, Section 2.2, Figure 2 (a-d**) and in **Supporting information, Section 3.2.**

The polymorphism in MFn at room temperature was investigated in the SAXS and WAXS range . From the WAXS results of MF1, in **Figure 5.(a)** the peaks at q=1.461 $Å^{-1}$ (d=4.3 Å) and q=1.583 $Å^{-1}$ (d=3.96 Å) are markers of the presence of a β' polymorph.[35,37] The MF1 SAXS pattern (**Figure 5.(b)**) displayed the presence a β'-2L phase melting completely at around 37 °C (see **Supporting Information, Section 2.3, Figure 3 (a)**). Sharp peaks were visible at q=0.149 $Å^{-1}$, q=0.297 $Å^{-1}$ and q=0.445 $Å^{-1}$, representing respectively the first, second and third order reflections of the same polymorph, with a d-spacing d=42.2 Å corresponding to a β'-2L structure.[33,34]

In the SAXS pattern of MF2 at 20°C (**Figure 5. (b)**) a complex peaks scheme indicated the presence of multiple phases, which were assigned to two β-2L forms arbitrarily called β-2L and β-2L(2), as

shown in **Supporting information, Section 3.4, Figure 4. (a).** The peak with the lowest q value (0.09 $Å^{-1}$) and d-spacing (68.9 Å) can be assigned to a β-3L form, whose third, fourth and fifth order peaks were also visible. The β-3L polymorph melted first at around 36°C. The two β-2L forms showed higher melting points of 42.5°C and 44°C (see **Supporting Information, Section 2.4, Figure 4 (a)**). The WAXS diffractogram of MF2 at equilibrium conditions (**Figure 5. (a)**) showed the presence of a sharp peak at 1.46 $Å^{-1}$, and other peaks of medium intensity at 1.37 $Å^{-1}$, 1.39 $Å^{-1}$ and at 1.54 $Å^{-1}$ associated to the β-3L form. The presence of other small peaks close to the characteristic β ones was indicative of the coexistence of the other β forms observed in the SAXS range.

At 20°C, MF3 showed evidence of the presence of two separate phases: a sharp peak at q=0.098 $Å^{-1}$, indicative of a β polymorph, can be distinguished in **Figure 5. (b)**, with d-spacing of 64.4 Å. This value was in accordance with the results of a previous study on SOS.[38] Peaks at q=0.194 $Å^{-1}$, q=0.291 $Å^{-1}$ and q=0.388 $Å^{-1}$ represented the second, third and fourth order reflections for this polymorph. However, the less intense but still evident peak at q=0.140 $Å^{-1}$ (d=44.9 Å) also suggested the presence of a β-2L phase, fully melted at 45°C (see **Supporting Information, Section 2.5 Figure 5 (a)**). This phase can be identified in the WAXS pattern of MF3 (**Figure 5. (a)**, peak at q=1.365 $Å^{-1}$, d=4.6. Å). SAXS at 20°C of the MF4 sample was then analysed and MF4 appeared only partially crystalline due to its low SFC at room temperature. As depicted in **Figure 5. (b)** the peaks at q=0.140 $Å^{-1}$ and q= 0.142 $Å^{-1}$ could be associated to the first reflection of two different lamellar phases. It is important to highlight that these two polymorphs, having different melting points, showed very similar d-spacing values (d=44.8 Å and d=44.3 Å), compatible with 2L structures, considering the TAGs composition of MF4. The WAXS diffractogram of MF4 (**Figure 5. (a)**), similarly to the SAXS, was mainly characterized by a broad baseline due to a considerable fraction of the mixture being still liquid. Two neat peaks with d-spacing of 46.2 Å and 45.7 Å respectively, indicated the presence of two immiscible β(2L) forms. These highly stable polymorphs can be attributed to the presence of tri-saturated TAGs (SSS, PPP) or 2L molecular compounds formed by specific pairs of TAGs (such as stochiometric

mixtures of PPO and POP or SSO and SOS). This was further confirmed by the high melting point of these polymorphs (47-48 °C).

MF2 and MF3 resemble more CB in terms of polymorphs nucleated, indeed a β-3L form was detected in both. MF4 molecular composition instead, seemed to lead preferentially to 2L structures. The absence of the β form in MF1 suggested that the transformation from the less stable β' polymorph to the more stable form occurs slower in this sample compared to the others. The reason of this difference is probably due to the higher content of POP. A slower transformation towards the β polymorphs in mixtures rich in POP was previously observed by Simone et al.[31] The absence of the β-3L form in MF1 and MF4 makes them potential good candidates for MF replacement.

Crystallization behavior studied with SAXS under controlled temperature profiles.

The crystallization behavior and polymorphic outcome of MF1 was investigated in situ, with SAXS. During the first crystallization profile performed at a cooling rate of -0.5°C/min (**Figure 6. (a)**), a peak at 0.133 $Å^{-1}$ (d=47 Å) appeared first at 20°C. Considering that MF1 is mainly composed of fatty acid chains with average length of 17.2 C atoms, this peak was assigned to a α-2L form. At lower temperature (7°C-8°C) another peak at a slightly higher d-spacing appeared (q=0.121 $Å^{-1}$, d=52 Å), suggesting the presence of another metastable 2L phase, starting to disappear at around 20°C upon heating. (**Figure 6.(a)**). The higher value of d-spacing means that this second phase originated from a fraction of MF1 containing TAGs with longer fatty acid chains compared to the α form previously nucleated, that are immiscible with those forming the first α-2L polymorph. Moreover, this phase nucleated and melted at a lower temperature compared to the first α-2L phase (7°C and 20°C respectively), which might be related to the higher degree of unsaturation of its forming TAGs (e-g-. OOP and OOS). The d-spacing and melting range of this metastable phase are compatible with the sub-α form reported in literature for cocoa butter[35]. These two immiscible 2L phases were named α (d=47 Å) and sub-α (d=52 Å) from now on, for clarity.

After a few minutes of holding at 5°C the peak at q=0.121 $Å^{-1}$ (sub-α) disappeared, while a peak at q=0.149 $Å^{-1}$ (associated to the β'-2L observed at room temperature) started to appear, indicating a polymorphic transformation from α to β'. In **Figure 6.(b)** the presence of the β'-2L phase is more evident in the third order reflection region, where the peaks of α-2L (q=0.4 $Å^{-1}$) and β'-2L (q= 0.44 $Å^{-1}$) do not overlap as the first order ones.

Upon heating at 0.5°C/min, the least stable α polymorphs melted completely at 22-23°C, whereas the peak of the β'-2L remained visible up to 36°C.[40]

MF1 was then cooled again down to 5°C, but this time with a faster cooling rate (-5°C/min). The results showed no significant difference compared to the slower cooling experiment, in terms of polymorphic behavior. The α-2L phase nucleated first at 17°C, then at 5°C the double chain sub-α appeared. Both phases nucleated at lower temperatures compared to the previous experiment. The difference in terms of crystallization temperatures in the two cooling processes is explained by the slower cooling rates providing more time for critical size nuclei to form; thus, slower cooling rates lead to nucleation at lower degrees of undercooling.[26]

Sample MF2 was as well recrystallized at a slow cooling rate of -0.5°C/min (**Figure 7. (a)**). The first peak (q=0.129 $Å^{-1}$, d=48.6 Å) was observed at around 23°C and it grew together with the second and third order reflections of the same phase, identified as the α form, similarly to MF1. During the cooling profile, another phase (q= 0.117 $Å^{-1}$, d= 53.5 Å) crystallised between 13 and 12°C; this is a sub-α form similarly to the one of MF1. In the last part of the cooling process, before reaching the target temperature of 5°C, the peaks of both these phases continued to increase in intensity, while shoulders from a more stable polymorph started to appear. Indeed, during the following holding profile (**Figure 7. (b)**), where the temperature was kept constant at 5°C, this third phase shoulders grew into peaks (first order peak q= 0.138 $Å^{-1}$, d= 45.5 Å) related to a more compact structure β'-2L form.[33] The **Supporting Information file, Section 3, Figures 1-6** reports graphs describing the association of the different scattering peaks of the same phase, as their q values are aligned in relation

to their Miller indices. Regarding the heating profile (**Figure 6. (c)**) α was observed melting at 25°C, while the sub-α was no longer visible, possibly covered by the β'-2L polymorph intense peaks, which were still partly visible above 40°C. The sample was completely melted at 45°C.

MF2 then underwent a second and faster cooling profile: the type and number of polymorphs identified were the same as the experiments at lower cooling rates, but some differences were observed. Firstly, nucleation happened at 18 °C, when peaks characteristic of the α form began to appear, while the sub-α phase started to form again at lower temperatures, becoming visible around 8 °C. At 0°C both α forms were still present and a third tri-layered form appeared. This polymorph is consistent with a γ-3L polymorph (d=75 Å), described previously by Mykhaylyk & Hamley for SOS.[38] This form completely melted before 20°C, and it is related to the high concentration of SOS in MF2.

The polymorphism during cooling crystallization of MF3 was investigated with SAXS. In **Figure 8. (a)** the significant patterns collected during the first cooling cycle at -0.5 °C/min are reported. A peak at q=0.120 $Å^{-1}$ started to form at 24°C (d=52.1 Å), which was associated to a α-2L form. This α-2L structure has a longer d-spacing (52.3 Å) than the one of the α-2L form of MF1 (d=47 Å). This may be explained by the presence of longer fatty acids in MF3 compared to MF1. Using the equation reported in the literature ($d = 2(1.27N_c) + 8)$)[26,41] to estimate the d-spacing of a mixture of TAGs with average chain length of 17.9 carbon atoms, a theoretical value of 53.4 Å is obtained, which is consistent with the experimental value of 52.1 Å.

With further cooling, at 15°C a shoulder at higher values of q started to form. Three separate phases became distinguishable at such temperature: a β'-2L (q=0.142 $Å^{-1}$, d=44.1 Å), already present at 20°C and two phases with overlapping peaks at q=0.166 $Å^{-1}$ and q=0.18 $Å^{-1}$ (**Figure 8. (a)**). These peaks are the second order reflections of two 3L structure with d-spacings of about 75 Å and 69 Å. These long-range d-spacings are likely belonging to a γ -3L and β'-3L phases respectively, which are typical

of SOS. [38] Mykhaylyk & Hamley[38] described them as intermediate phases, in terms of stability, between α-2L and β -3L; these polymorphs were also reported in other studies.[42,43,44] After 15 minutes of holding MF3 at 5° C, a peak at q=0.095 $Å^{-1}$ (d=65.9 Å), which can be related to the β-3L phase became visible (**Figure 8. (b)**). This confirms that in MF3 the transformation to the most stable polymorph occurred more rapidly compared to MF1, which did not show signs of β-3L form during the cooling and isothermal holding processes. Upon heating at 0.5°C/min, the least stable α-2L polymorph disappeared first at 20°C (**Figure 8. (c)**). This phase nucleated at 24°C, so the fact that its peak disappeared at 20°C indicated its transformation into the more stable β'-2. In the temperature range of 10-30° C the intensity of the γ peaks progressively decreased, probably because this phase started to convert into a more stable form. The β'-3L phase melted between 32°C and 34°C, whereas the β-3L peak persisted up to 38°C. A peak corresponding to a 2L phase was still visible at 40°C. This is probably a β-2L polymorph generated by a fraction of high melting TAGs (e.g., tri-saturated such as SSS), which could not be identified before because of the overlapping with the peaks of the more unstable forms. [45,46]

After the sample was fully melted upon the first crystallization cycle, another one was performed, with a faster cooling rate of -5°C/min (see **Supporting Information, Section 2.5, Figure 5. (e)**). The results in this case were similar to MF1: the α-2L phase (d=52.3 Å) nucleated first, between 23°C and 18°C, at a lower temperature compared to the previous cycle. Then a sub-α phase, with a higher d spacing (d=55.5 Å), not observed in the previous crystallization cycle, appeared between 13°C and 8°C. This sub-α polymorph remained during the holding period at 5°C, when the β'-2L characteristic first order peak started to be evident. In this case neither the γ nor the β'-3L phases were observed.

For MF4 a first cooling ramp led to the formation of numerous peaks, as shown in **Figure 9. (a)** The first peak (q=0.124 $Å^{-1}$, d=50.5 Å) became visible at around 24°C and it was attributed to an α phase, which kept growing until the sub-α appeared at 10.9°C (q= 0.019 $Å^{-1}$, d= 52.8 Å), with two sharp

peaks corresponding to the first and second order reflections together with the fourth order peak that became visible as the cooling process proceeded. At 10.9°C shoulders started to be visible on the right of the first peak at q=0.07Å^{-1}. However, they did not fully develop during the cooling ramp and the following 10 minutes holding; thus, the discrimination of the corresponding phases is not trivial. MF4 was then kept at 5°C for longer than the other samples (around 50min). **Figure 9. (b)** shows the differences between the patterns during this long period of holding. The α form crystallized at higher temperature disappeared due to its instability. The sub-α phase decreased as well, even though its peaks were still observed for longer compared to α. On the other hand, the shoulders that were observed at the end of the slow cooling ramp grew into two overlapping peaks centred at around q=0.14 Å^{-1}. At the end of the holding time four different polymorphs could be distinguished. A first one was the sub-α form originated during cooling, while overlapping peaks from an unstable γ-3L form[38] and a more stable β-2L developed after 15 minutes at 5°C. Finally, weaker shoulders assigned to a β'-3L[38] polymorph were observed after ~25minutes. The appearance of γ-3L and β'-3L after a longer time at 5 °C is due to the relatively large amount of SOS in MF 4.

The following heating process provided a better understanding of the type and number of phases formed at 5°C. In **Figure 9. (c)** the weak shoulders representing the β'-3L polymorph were already decreased between 10°C and 13°C and completely melted before 22°C. Peaks from the α forms fully disappeared before 13°C, coherently with the instability typical of this polymorph. The tri-layered γ-form seemed completely melted before 22°C. At this temperature only the most stable β-2L form was still visible and kept growing. At 40°C the last trace of a first order β-2L peak was the only one still detectable (**Figure 9. (b)**).

The dynamic study of crystallization was again repeated applying a faster cooling rate. At 5°C only the two α forms were visible and their crystallization temperatures were lowered of several degrees compared to the slower cooling profile, as the first peak was observed at 20°C instead of 24°C and the second phase peaks appeared at 10°C.

20% blends of MF and MFn in CB

To investigate how the addition of MF or MF*n* to CB affects its crystallization behaviour, mixtures with 20% in mass of MF, MF1, MF2, MF3 and MF4 were prepared and analysed at room temperature after one week with both PXRD and SAXS.

PXRD diffractograms of the mixtures did not show significant differences compared to pure CB. The wide-angle patterns reported in **Figure 10. (a)** showed a sharp peak with d=4.6 Å and four less intense peaks at higher values of q. The values of d-spacing of these minor peaks were identical to CB in all the blends (d=3.97 Å, 3.87 Å, 3.74 Å and 3.64 Å) and they were all indicative of the presence of the β(V) polymorph of CB.

As depicted in **Figure 10. (b)** at 20 °C the mixtures MF1 20% **(brown)** MF2 20% **(green)**, and MF3 20% **(blue)** showed a similar SAXS pattern to the one of pure CB (**black**). The peaks of the β-3L phases are superimposable with the ones of CB, whereas the peaks of the β-2L phases seem different, as they are associated to the presence of different minor TAGs.

In the SAXS pattern of the MF 20% blend (**Figure 10. (b)**), the peaks related to a β-2L form (q=0.143 $Å^{-1}$, q=0.428 $Å^{-1}$) are noticeable. The intensity of the β(V) peaks was lower compared to CB and the other mixtures, with shifted d-spacing (MF 20% d=66.1 CB d=63.9).When the MF 20% blend was heated, the β-3L phase melted between 32°C and 34° C, earlier than the β-2L, whose peak persisted up to 38°C. A melting temperature of about 33°C is consistent with the values reported in the literature for the β(V) form of milk chocolate.[47] A similar behaviour is observed in MF4 20% (**Figure 10. (pink))** that shows the most similar diffraction pattern to MF 20%, compared to the other mixtures analysed in this work. This may be ascribed to the lower crystallinity of these two mixtures and to the very low SFC of the pure MF4 (17% at 25°C, 25% at 20°C), rather than similarities in polymorphic behaviour**.** The X-ray diffraction patterns of mixture MF2 20% and MF3 20% were more similar to pure CB than to MF 20%, which is consistent with what was observed in the pure compounds. Also MF1 20% seemed more similar to CB alike the aforementioned blends, even though pure MF1 behaved differently from CB in terms of polymorphic contribution at room temperature.

Regarding the SAXS experiments performed with temperature profiles, it was observed that the number and types of polymorphs nucleated in MF 20% and MF*n* 20% was the same as CB.

Indeed, SAXS patterns of all mixtures resembled very much CB patterns in terms of polymorphic contribution and crystallization/melting behaviour, with variations on melting and nucleation temperatures in a range of ± 2°C. The peculiar composition of each MF*n* did not bring to the blend any detectable difference in terms of number and types of polymorphs nucleated.

SAXS patterns collected during cooling, holding, and heating profiles for all the mixtures are reported in **Supporting info, Section 2.7, Figure. 7-11.**

HS-PLM analysis of the crystalline microstructure and crystallization

Hot stage polarized light microscopy (HS-PLM) was used to study the microstructure of the crystallized fat mixtures. Two separate crystallization experiments, at different cooling rates, were performed in order to evaluate the effect of the cooling rate on the crystal morphology which appeared composed of needle-shaped crystalline aggregates. At the end of the cooling crystallization a dense network of crystals was formed. **Figure 11. (a)** shows frames taken during the crystallization experiment performed at -0.5° C/min and their corresponding binarization.

The cooling rate does not seem to have a significant effect on the appearance of the CB microstructure.

Graphs reporting the number of white pixels as a function of time during the cooling crystallization experiment at a rate of -0.5°C/min are shown in **Figure 12.** For each curve a similar trend is noticeable, with a "increase-plateau-increase" profile. The curve related to CB (**Figure 12. (a) (green)**) showed a rapid increase of the number of white pixels at about 23°C, corresponding to nucleation of the α-2L crystals, then the curve presented a constant slope up to 15°C. At this point the curve became steeper, indicating the nucleation of another phase, most likely the β'-2L (observed at 14°C in the SAXS experiments). In the MF curve the first nucleation event occurred at 22°C. Then, at 20°C the curve slope increased slightly and at about 14°C crystalline aggregates with more

elongated shape started to develop, as shown in **Figure 11. (b)**. It is possible that the first crystals that nucleated were those of the α-2L form, whereas the fraction that crystallized at 14°C were α-3L,which is consistent with what observed by Pratama et al.[26,47]. Below 10°C the slope of the curve increased more drastically, as the crystal aggregates seemed to change shape (**Figure 11. (b)**). In the SAXS patterns a transformation from α-3L to β'-3L was observed below 10°C during the crystallization at -0.5°C/min (**Supporting Information file, Section 1.2, Figure 1.2 (b)**). It is possible that the increase in slope of the curve of white pixels refers to this polymorphic transformation.

In the MF1 curve (**Figure 12. (a) (black)**) after the nucleation of the α-2L phase at 20°C, the number of white pixels increased linearly, with a steeper slope from 8 °C. This last increase in number of white pixels possibly refers to the crystallization of the sub-α phase.

The α-2L phase of MF3 nucleated at 26°C. After a first rapid increase, the curve related to the number of white pixels (**Figure 12. (a) (pink)**) showed a less steep slope up to 16°C. At this temperature a second rapid increase in number of white pixels was observed. At 15°C a β'-2L phase appeared during the SAXS analysis with the same cooling rate of -0.5°C/min. Thus, it is possible that the change in slope at 16°C indicates the transformation from α-2L to β'-2L. No visible differences were noticed later in the shape of the crystalline aggregates, as shown in **Figure 13. (c)**.

MF2 (**Figure 12. (a) (brown)**) underwent two sharp crystallization steps at ~22°C and ~12°C likely related to a polymorphic transformation. Indeed, as it is possible to observe in **Figure 13. (b)**, MF2 firstly showed few spherical agglomerates at 22°C, increasing in number and in size in the second stage of nucleation at around 12°C, until a compact crystal network was obtained.

MF4 (**Figure 12. (a) (blue)**) sample started crystallizing above 25°C and behaved slightly differently from the previous ones. Elongated crystalline aggregates formed and initially grew without any spherical structure formation, as it is possible to notice in **Figure 13. (c).** Later, it was possible to see wider spherical agglomerates in the background, coexisting with the needles. This was suggesting the coexistence of at least two immiscible crystal phases forming at different temperatures (possibly the

α and a more stable β form). MF4 profile indicates a less steep change of slope compared to the other samples.

Figure 12. (b). reports the trends observed for the mixtures of MF*n* with CB. In terms of crystalline microstructure, no significant difference from pure CB was observed, and the appearance of the sample matrix became visually homogeneous when crystallization was complete. **Figure 14**. shows frames taken at the end of the crystallization experiment (-0.5°C/min) for CB and each 20% mixture for the sake of comparison.

It is clearly noticeable that the shape of crystalline aggregates in the mixtures resemble very much the ones of CB. Main difference was observed after the binarization process and the data plot, indeed the total number of white pixels per unit area in the case of MF1 20% and MF3 20% appeared lower compared to the other blends. Additionally, the white pixels profile does not seem to follow the "increase-plateau-increase" trend observed for the pure components and the other mixtures. MF2 20% and MF4 20% crystallization profile appeared to be closer to MF 20%, both in number of pixels and in the white pixels trend.

Differential scanning calorimetry

The DSC events with onsets and offsets observed during the cooling/heating ramp at ±2°C/min are reported schematically in **Table 6** for CB, MF,and MF*n* and all DSC curves are collected in the **Supporting information file, Section 4.**

For all samples the cooling rate applied did not seem to affect the number of thermal events observed, slight changes in the onset temperature were observed, as observed also during the SAXS experiments.

The DSC curves obtained via cooling of CB showed two main exothermic peaks. The first thermal even started at 21°C in the slower crystallization and at 20° C in the faster one. During the heating ramp, three endothermic events occurred, although their peaks seem to be partly overlapping. These

events may be attributed to the melting of the α and sub-α polymorphs, subsequently followed by the melting of a more stable structure, possibly the β' form.

For MF it is possible to distinguish two exothermic events during both the cooling profiles. The first started at about 20°C in the slower crystallization profile and at 18°C in the faster one. This first exothermic event may be associated to the nucleation of the MF α-2L phase. The second major peak onset is recorded at 12°C in the cooling at -2°C/min and at a slightly lower temperature for the faster cooling profile. This exothermic event may refer to the crystallization of the less stable α-3L phase observed in the SAXS patterns. Between the two major exothermic events another smaller and less defined peak appeared in the range 16°C-12°C.

The melting curve of MF does not have a clear baseline and the first peak in the range 0°C-11°C is not easy to resolve. In the range 12°C-17°C two overlapping peaks are visible, probably indicating the melting of the α-3L phases. The last broad peak at higher temperature (from 17°C to 36 °C) probably represents the melting of the α-2L phase and a more stable β'-2L form. The latter melted at 36°C also in the SAXS analysis.

In the DSC curve of MF1 two exothermic peaks are visible. Both exothermic peaks are possibly associated with the crystallization of α and sub-α phases. The first nucleated at about 19°C-18°C depending on the cooling rate applied, whereas the second peak started at 10°C. A weak peak at temperature below zero (-2°C to -5°C) is visible and it probably represents the crystallization of a low melting fraction of MF1 (e.g., containing polyunsaturated TAGs). The melting curve shows several overlapping events in the range 5°C-22°C. Eventually these enlarged overlapping events could be attributed to the melting of the two α phases and possibly of the more stable β'.

The thermograms of MF2 are consistent with the SAXS data. The first thermal event occurred in the range 22°C-18°C while a second one can be observed at around 15°C, ending at 5°C. Upon heating, a broad melting peak was observed, indicating a wide polymorphic composition (α-2L phases and β'-2L), as supported by the SAXS experiments.

The first exothermic event in the DSC curve of MF3 started at about 24°C for the slower cooling rate and at 22°C in the faster cooling profile. These temperatures are in accordance with the SAXS patterns for the α-2L forms crystallization range. The second exothermic peak started at 15°C in both the cooling ramps. The onset temperature of this second exothermic event could suggest the crystallization of a β'-2L phase, not distinguishable by the following nucleation event (possibly γ-3L and β' 3L- as it was found in SAXS). A distinct exothermic event, which started at 10°C and ended at about 25°C, occurred during heating and is indicative of a polymorphic transition. Two minor exothermic events happened at low temperature (5°C and -7°C) and two endothermic events also occurred at slightly higher temperatures (7°C and -4°C); they can be attributed to the crystallization temperature and melting of the low melting fractions of MF3. The presence of these low melting fractions, composed of polyunsaturated TAGs, might have an enhancing effect on the subsequent polymorphic transformation, A broad peak was also visible at high temperatures (up to 38°C), probably indicating the melting of the β-3L and β-2L phases, already observed during the SAXS analysis.

The MF4 sample, showed a complex DSC profile, similarly to MF. Indeed, both samples possess a wide range of TAGs and a low melting TAGs fraction that remains liquid in the temperature range of the analysis. However, the first step of crystallization appeared in the range 24°C-17°C, similarly to MF3 and even in this case this temperature range is in accordance with the SAXS data for the nucleation of the α-2L and sub-α forms. A second exothermic event characterized by a broad peak started at 15°C in both the cooling profiles. Possibly in this range of temperature we observed the nucleation of the β'-2L, γ-3L and β' 3L, as seen during the SAXS experiments. During the heating ramp an exothermic event, which started at 10°C and ended at about 28°C, was observed: this corresponds to a polymorphic transition from the more metastable forms to the more stable ones. The melting range for MF4 is very wide, between 28 and 42°C, due to MF4 complex TAGs composition.

The thermal profiles of the MFn 20% blends, including MF20%, are very similar to pure CB: **Table 7.** reports the temperatures and ranges of the endothermic and exothermic peaks observed. Nevertheless, some differences were noticeable especially in MF 20%, MF3 20% and MF4 20%, which possess a broader melting range compared to CB, starting at lower temperatures (e.g. MF 20%= 5°C-25°C, MF3 20% = 5°C- 29°C, MF4 20%= 4°C-28°C).

CONCLUSIONS

This work investigated the crystallization behavior of four plant based triacylglycerides mixtures (MF*n*) to be used as milk replacements in vegan chocolate, and their 20% w/w blends with a sample of cocoa butter of Ghanian origin. The effectiveness of these mixtures of fats to emulate the crystallization behavior of milk fat when mixed with cocoa butter was investigated. The TAGs composition of each mixture was estimated and compared to that of milk fat and cocoa butter, to understand whether the thermal behavior, crystalline forms and microstructure of milk fat can be replicated with fat mixtures with different TAGs composition. It was observed that the samples MF2 and MF3 and their 20% mixture perform similarly to CB in terms of crystallization behavior, and consequently they do not seem suitable as milk fat replacers. This observation was in accordance to the TAGs composition of MF2 and MF3 that, as reported in **Table 4** and **5**, resembles the one of CB more closely compared to the other samples. MF3 behavior appeared slightly different, possibly due to the high disproportion in composition between POP (<1%) and SOS (>37%), and a higher percentage of unsaturated FA (as reported in **Table 4** and **5**), giving to this sample a softer and creamy texture (SFC% at 20°C=37%). MF4 appeared different from CB in terms of crystallization characteristics due to the high variety of TAGs contained in this sample, and its general trend can be considered closer to the one of MF. The 20% mixture of MF4 with CB is the most similar to MF 20% in terms of structure and thermal behavior, despite the differences in composition between MF and MF4. Indeed MF4 has a low SFC% at room temperature (25% at 20°C), giving it a soft texture and a

creamy appearance and a high percentage of unsaturated FA, which replicate the crystallization behavior of MF when mixed with CB. MF1, having a 42.4 % of its total composition made of POP (see **Table 4**), tends to differ from CB polymorphic behavior. Indeed, it remains longer in unstable β' form compared to the other samples. The large amount of relatively long, saturated FA does not make MF1 an ideal MF replacer.

In conclusion, this study emphasizes the significant correlation between the composition of TAGs, the crystallization thermodynamic, kinetics, and the crystalline microstructure of edible fats. Hence, the solid-state landscape that can be achieved by blending different TAGs mixtures is worth exploring, together with and the resulting thermal and mechanical properties. This knowledge is essential to overcome the challenge of finding suitable substitutes of animal fats in confectionary products. Plant-based fats represent an emerging frontier in the chocolate industry, offering numerous advantages to finished products. For individuals with lactose intolerance, traditional chocolate formulations containing milk derivatives pose difficulties, while another significant category of consumers opt for vegan lifestyles, which diverge from conventional milk chocolate compositions. The insight provided by this work may be crucial for chocolate producers seeking to incorporate plant-based triacylglycerides mixtures in chocolate products as cow milk fat replacers.

ACKNOWLEDGEMENTS

This project received funding from the European Research Council (ERC) under the European Union's Horizon 2020 research and innovation programme (grant agreement no. 949229). We acknowledge Diamond Light Source (DLS), CERIC and ESRF for beamtime on beamlines I22, SAXS and ID02 under proposals SM34844-1 (DLS), 20222033 (CERIC), and SC 5464 (ESRF). Finally, we are grateful to beamline scientists Prof. Nick Terrill and Dr Andrew Smith (DLS), Dr William Chevremont (ESRF), Dr Barbara Sartori and Dr Sigrid Bernstorff (CERIC, Elettra Sincrotrone Trieste) for the help and support with the three SAXS beamlines and special setups used

for the work. Raw data collected on beamline ID02 at ESRF can be accessed at the DOI: 10.15151/ESRF-ES-1353618911.

6. FORMATTING OF FUNDING SOURCES

ERC Starting Grant 949229.

Diamond Light Source (UK) standard peer-reviewed access.

ESRF (France) standard peer-reviewed access.

Elettra Sincrotrone Trieste (Italy) standard CERIC peer-reviewed access.

REFERENCES

(1) Talbot, G. Chocolate and Cocoa Butter—Structure and Composition. In *Cocoa Butter and Related Compounds*; AOCS Press, 2012; pp 1–33. https://doi.org/10.1016/B978-0-9830791-2-5.50004-9.

(2) Jahurul, M. H. A.; Zaidul, I. S. M.; Norulaini, N. A. N.; Sahena, F.; Jinap, S.; Azmir, J.; Sharif, K. M.; Mohd Omar, A. K. Cocoa Butter Fats and Possibilities of Substitution in Food Products Concerning Cocoa Varieties, Alternative Sources, Extraction Methods, Composition, and Characteristics. *J. Food Eng.* **2013**, *117* (4), 467–476. https://doi.org/10.1016/J.JFOODENG.2012.09.024.

(3) Huyghebaert, A.; Verhaeghe, D.; De Moor, H. Fat Products Using Chemical and Enzymatic Interesterification. In *Fats in Food Products*; Springer, Boston, MA, 1994; pp 319–345. https://doi.org/10.1007/978-1-4615-2121-1_9.

(4) Pease, J. J. Confectionery Fats from Palm Oil and Lauric Oil. *J. Am. Oil Chem. Soc.* **1985**, *62*

(2), 426–430. https://doi.org/10.1007/BF02541416.

(5) Jacobsberg, B.; Oh Chuan Ho. Studies in Palm Oil Crystallization. *J. Am. Oil Chem. Soc.* **1976**, *53* (10), 609–617. https://doi.org/10.1007/BF02586272.

(6) Kang, K. K.; Jeon, H.; Kim, I. H.; Kim, B. H. Cocoa Butter Equivalents Prepared by Blending Fractionated Palm Stearin and Shea Stearin. *Food Sci. Biotechnol.* **2013**, *22* (2), 347–352. https://doi.org/10.1007/S10068-013-0087-8.

(7) Norazlina, M. R.; Jahurul, M. H. A.; Hasmadi, M.; Mansoor, A. H.; Norliza, J.; Patricia, M.; Ramlah George, M. R.; Noorakmar, A. W.; Lee, J. S.; Fan, H. Y. Trends in Blending Vegetable Fats and Oils for Cocoa Butter Alternative Application: A Review. *Trends Food Sci. Technol.* **2021**, *116*, 102–114. https://doi.org/10.1016/J.TIFS.2021.07.016.

(8) Ewens, H.; Metilli, L.; Simone, E. Analysis of the Effect of Recent Reformulation Strategies on the Crystallization Behaviour of Cocoa Butter and the Structural Properties of Chocolate. *Curr. Res. Food Sci.* **2021**, *4*, 105–114. https://doi.org/10.1016/J.CRFS.2021.02.009.

(9) Devos, N.; Reyman, D.; Sanchez-Cortés, S. Chocolate Composition and Its Crystallization Process: A Multidisciplinary Analysis. *Food Chem.* **2021**, *342*, 128301. https://doi.org/10.1016/J.FOODCHEM.2020.128301.

(10) Afoakwa, E. O.; Paterson, A.; Fowler, M.; Vieira, J. Influence of Tempering and Fat Crystallization Behaviours on Microstructural and Melting Properties in Dark Chocolate Systems. *Food Res. Int.* **2009**, *42* (1), 200–209. https://doi.org/10.1016/j.foodres.2008.10.007.

(11) Lonchampt, P.; Hartel, R. W. Fat Bloom in Chocolate and Compound Coatings. *Eur. J. Lipid Sci. Technol.* **2004**, *106* (4), 241–274. https://doi.org/10.1002/EJLT.200400938.

(12) Altimiras, P.; Pyle, L.; Bouchon, P. Structure-Fat Migration Relationships during Storage of

Cocoa Butter Model Bars: Bloom Development and Possible Mechanisms. *J. Food Eng.* **2007**, *80* (2), 600–610. https://doi.org/10.1016/j.jfoodeng.2006.06.022.

(13) Chaiseri, S.; Dimick, P. S. Dynamic Crystallization of Cocoa Butter. I. Characterization of Simple Lipids in Rapid- and Slow-Nucleating Cocoa Butters and Their Seed Crystals. *J. Am. Oil Chem. Soc.* **1995**, *72* (12), 1491–1496. https://doi.org/10.1007/BF02577842.

(14) Foubert, I.; Vanrolleghem, P. A.; Thas, O.; Dewettinck, K. Influence of Chemical Composition on the Isothermal Cocoa Butter Crystallization. *J. Food Sci.* **2004**, *69* (9), E478–E487. https://doi.org/10.1111/J.1365-2621.2004.TB09933.X.

(15) Chaiseri, S.; Dimick, P. S. Lipid and Hardness Characteristics of Cocoa Butters from Different Geographic Regions. *J. Am. Oil Chem. Soc.* **1989**, *66* (12), 1771–1776. https://doi.org/10.1007/BF02660745.

(16) Lehrian, D. W.; Keeney, P. G.; Butler, D. R. Triglyceride Characteristics of Cocoa Butter from Cacao Fruit Matured in a Microclimate of Elevated Temperature1. *J. Am. Oil Chem. Soc.* **1980**, *57* (2), 66–69. https://doi.org/10.1007/BF02674362.

(17) Shukla, V. K. S.; Schiøtz Nielsen, W.; Batsberg, W. A Simple and Direct Procedure for the Evaluation of Triglyceride Composition of Cocoa Butters by High Performance Liquid Chromatography - A Comparison with the Existing TLC-GC Method. *Fette, Seifen, Anstrichm.* **1983**, *85* (7), 274–278. https://doi.org/10.1002/LIPI.19830850705.

(18) J. Bricknell, R. W. H. Relation of Fat Bloom in Chocolate to Polymorphic Transition of Cocoa Butter. *J. Am. Oil Chem. Soc.* **1998**, *75*, 1609–1616.

(19) Lohman, M. H.; Hartel, R. W. Effect of Milk Fat Fractions on Fat Bloom in Dark Chocolate. *J. Am. Oil Chem. Soc.* **1994**, *71* (3), 267–276. https://doi.org/10.1007/BF02638052.

(20) Campbell, L. B.; Andersen, D. A.; Keeney, P. G. Hydrogenated Milk Fat as an Inhibitor of

the Fat Bloom Defect in Dark Chocolate. *J. Dairy Sci.* **1969**, *52* (7), 976–979. https://doi.org/10.3168/JDS.S0022-0302(69)86678-6.

(21) Pajin, B.; Jovanovic, O. Influence of High-Melting Milk Fat Fraction on Quality and Fat Bloom Stability of Chocolate. *Eur. Food Res. Technol.* **2005**, *220* (3–4), 389–394. https://doi.org/10.1007/S00217-004-1077-0.

(22) Waldron, D. S.; Hoffmann, W.; Buchheim, W.; McMahon, D. J.; Goff, H. D.; Crowley, S. V.; Moloney, C.; O'regan, J.; Giuffrida, F.; Torres, I. C.; Siong, P. Role of Milk Fat in Dairy Products. *Adv. Dairy Chem. Vol. 2 Lipids, Fourth Ed.* **2020**, *2*, 245–305. https://doi.org/10.1007/978-3-030-48686-0_9.

(23) Tietz, R. A.; Hartel, R. W. Effects of Minor Lipids on Crystallization of Milk Fat-Cocoa Butter Blends and Bloom Formation in Chocolate. *JAOCS, J. Am. Oil Chem. Soc.* **2000**, *77* (7), 763–771. https://doi.org/10.1007/S11746-000-0122-5/METRICS.

(24) Bahari, A.; Akoh, C. C. Texture, Rheology and Fat Bloom Study of 'Chocolates' Made from Cocoa Butter Equivalent Synthesized from Illipe Butter and Palm Mid-Fraction. *LWT* **2018**, *97*, 349–354. https://doi.org/10.1016/j.lwt.2018.07.013.

(25) Biswas, N.; Cheow, Y. L.; Tan, C. P.; Kanagaratnam, S.; Siow, L. F. Cocoa Butter Substitute (CBS) Produced from Palm Mid-Fraction/Palm Kernel Oil/Palm Stearin for Confectionery Fillings. *JAOCS, J. Am. Oil Chem. Soc.* **2017**, *94* (2), 235–245. https://doi.org/10.1007/S11746-016-2940-4.

(26) Pratama, Y.; Simone, E.; Rappolt, M. The Unique Crystallization Behavior of Buffalo Milk Fat. *Cryst. Growth Des.* **2021**, *21* (4), 2113–2127. https://doi.org/10.1021/ACS.CGD.0C01543/ASSET/IMAGES/LARGE/CG0C01543_0008.JPEG.

(27) Gresti, J.; Bugaut, M.; Maniongui, C.; Bezard, J. Composition of Molecular Species of Triacylglycerols in Bovine Milk Fat. *J. Dairy Sci.* **1993**, *76* (7), 1850–1869. https://doi.org/10.3168/JDS.S0022-0302(93)77518-9.

(28) Metin, S.; Hartel, R. W. Milk Fat and Cocoa Butter. In *Cocoa Butter and Related Compounds*; AOCS Press, 2012; pp 365–392. https://doi.org/10.1016/B978-0-9830791-2-5.50018-9.

(29) Nagy, K.; Sandoz, L.; Destaillats, F.; Schafer, O. Mapping the Regioisomeric Distribution of Fatty Acids in Triacylglycerols by Hybrid Mass Spectrometry. *J. Lipid Res.* **2013**, *54*. https://doi.org/10.1194/jlr.D031484.

(30) Zeb, A.; Murkovic, M. Analysis of Triacylglycerols in Refined Edible Oils by Isocratic HPLC-ESI-MS. *Eur. J. Lipid Sci. Technol.* **2010**, *112* (8), 844–851. https://doi.org/10.1002/EJLT.201000064.

(31) Simone, E.; Rappolt, M.; Ewens, H.; Rutherford, T.; Marty Terrade, S.; Giuffrida, F.; Marmet, C. A Synchrotron X-Ray Scattering Study of the Crystallization Behavior of Mixtures of Confectionary Triacylglycerides: Effect of Chemical Composition and Shear on Polymorphism and Kinetics. *Food Res. Int.* **2024**, *177*, 113864. https://doi.org/10.1016/J.FOODRES.2023.113864.

(32) Ghazani, S. M.; Marangoni, A. G. The Triclinic Polymorphism of Cocoa Butter Is Dictated by Its Major Molecular Species, 1-Palmitoyl, 2-Oleoyl, 3-Stearoyl Glycerol (POS). *Cryst. Growth Des.* **2019**, *19* (1), 90–97. https://doi.org/10.1021/ACS.CGD.8B00973/ASSET/IMAGES/LARGE/CG-2018-00973Y_0004.JPEG.

(33) Bresson, S.; Lecuelle, A.; Bougrioua, F.; El Hadri, M.; Baeten, V.; Courty, M.; Pilard, S.; Rigaud, S.; Faivre, V. Comparative Structural and Vibrational Investigations between Cocoa

Butter (CB) and Cocoa Butter Equivalent (CBE) by ESI/MALDI-HRMS, XRD, DSC, MIR and Raman Spectroscopy. *Food Chem.* **2021**, *363*, 130319. https://doi.org/10.1016/J.FOODCHEM.2021.130319.

(34) El Hadri, M.; Bresson, S.; Lecuelle, A.; Bougrioua, F.; Baeten, V.; Nguyen, V. H.; Faivre, V.; Courty, M. Structural and Vibrational Investigations of Mixtures of Cocoa Butter (CB), Cocoa Butter Equivalent (CBE) and Anhydrous Milk Fat (AMF) to Understand Fat Bloom Process. *Appl. Sci. 2022, Vol. 12, Page 6594* **2022**, *12* (13), 6594. https://doi.org/10.3390/APP12136594.

(35) Bresson, S.; Rousseau, D.; Ghosh, S.; El Marssi, M.; Faivre, V. Raman Spectroscopy of the Polymorphic Forms and Liquid State of Cocoa Butter. *Eur. J. Lipid Sci. Technol.* **2011**, *113* (8), 992–1004. https://doi.org/10.1002/EJLT.201100088.

(36) Loisel, C.; Keller, G.; Lecq, G.; Bourgaux, C.; Ollivon, M. Phase Transitions and Polymorphism of Cocoa Butter. *JAOCS, J. Am. Oil Chem. Soc.* **1998**, *75* (4), 425–439. https://doi.org/10.1007/S11746-998-0245-Y/METRICS.

(37) Grotenhuis, E. Ten; Van Aken, G. A.; Van Malssen, K. F.; Schenk, H. Polymorphism of Milk Fat Studied by Differential Scanning Calorimetry and Real-Time X-Ray Powder Diffraction. *J. Am. Oil Chem. Soc.* **1999**, *76* (9), 1031–1039. https://doi.org/10.1007/S11746-999-0201-5.

(38) Mykhaylyk, O. O.; Hamley, I. W. The Packing of Triacylglycerols from SAXS Measurements: Application to the Structure of 1,3-Distearoyl-2-Oleoyl-Sn-Glycerol Crystal Phases. *J. Phys. Chem. B* **2004**, *108* (23), 8069–8083. https://doi.org/10.1021/JP0379704/ASSET/IMAGES/LARGE/JP0379704F00016.JPEG.

(39) Campos, R.; Ollivon, M.; Marangoni, A. G. Molecular Composition Dynamics and Structure of Cocoa Butter. *Cryst. Growth Des.* **2010**, *10* (1), 205–217.

https://doi.org/10.1021/CG900853E/ASSET/IMAGES/LARGE/CG-2009-00853E_0016.JPEG.

(40) Berry, S. E. E. Triacylglycerol Structure and Interesterification of Palmitic and Stearic Acid-Rich Fats: An Overview and Implications for Cardiovascular Disease. *Nutr. Res. Rev.* **2009**, *22* (1), 3–17. https://doi.org/10.1017/S0954422409369267.

(41) Ladd Parada, M.; Sadeghpour, A.; Vieira, J.; Povey, M.; Rappolt, M. Global Small-Angle X-Ray Scattering Data Analysis of Triacylglycerols in the α-Phase (Part II). *J. Phys. Chem. B* **2018**, *122* (45), 10330–10336. https://doi.org/10.1021/ACS.JPCB.8B06708/ASSET/IMAGES/MEDIUM/JP-2018-067083_0006.GIF.

(42) Himawan, C.; Starov, V. M.; Stapley, A. G. F. Thermodynamic and Kinetic Aspects of Fat Crystallization. *Adv. Colloid Interface Sci.* **2006**, *122* (1–3), 3–33. https://doi.org/10.1016/J.CIS.2006.06.016.

(43) Ueno, S.; Minato, A.; Yano, J.; Sato, K. Synchrotron Radiation X-Ray Diffraction Study of Polymorphic Crystallization of SOS from Liquid Phase. *J. Cryst. Growth* **1999**, *198–199* (pt 2), 1326–1329. https://doi.org/10.1016/S0022-0248(98)01018-5.

(44) Ladd Parada, M.; Sadeghpour, A.; Vieira, J.; Povey, M.; Rappolt, M. Global Small-Angle X-Ray Scattering Data Analysis of Triacylglycerols in the α-Phase (Part II). *J. Phys. Chem. B* **2018**, *122* (45), 10330–10336. https://doi.org/10.1021/ACS.JPCB.8B06708/ASSET/IMAGES/MEDIUM/JP-2018-067083_0006.GIF.

(45) Sato, K.; Ueno, S. Polymorphism in Fats and Oils. *Bailey's Ind. Oil Fat Prod.* **2005**. https://doi.org/10.1002/047167849X.BIO020.

(46) Bayés-García, L.; Sato, K.; Ueno, S. Polymorphism of Triacylglycerols and Natural Fats. *Bailey's Ind. Oil Fat Prod.* **2020**, 1–49. https://doi.org/10.1002/047167849X.BIO020.PUB2.

(47) Pratama, Y.; Burholt, S.; Baker, D. L.; Sadeghpour, A.; Simone, E.; Rappolt, M. Polymorphism of a Highly Asymmetrical Triacylglycerol in Milk Fat: 1-Butyryl 2-Stearoyl 3-Palmitoyl-Glycerol. *Cryst. Growth Des.* **2022**, *22* (10), 6120–6130. https://doi.org/10.1021/ACS.CGD.2C00713/ASSET/IMAGES/LARGE/CG2C00713_0008.JPEG.

(48) Gregersen, S. B.; Miller, R. L.; Hammershøj, M.; Andersen, M. D.; Wiking, L. Texture and Microstructure of Cocoa Butter Replacers: Influence of Composition and Cooling Rate. *Food Struct.* **2015**, *4*, 2–15. https://doi.org/10.1016/J.FOOSTR.2015.03.001.

(49) Herrera, M. L.; Hartel, R. W. Effect of Processing Conditions on Physical Properties of a Milk Fat Model System: Microstructure. *J. Am. Oil Chem. Soc.* **2000**, *77* (11), 1197–1205. https://doi.org/10.1007/S11746-000-0186-2.

(50) Campos, R.; Narine, S. S.; Marangoni, A. G. Effect of Cooling Rate on the Structure and Mechanical Properties of Milk Fat and Lard. *Food Res. Int.* **2002**, *35* (10), 971–981. https://doi.org/10.1016/S0963-9969(02)00159-X.

(51) Sato, K.; Bayés-García, L.; Calvet, T.; Cuevas-Diarte, M. À.; Ueno, S. External Factors Affecting Polymorphic Crystallization of Lipids. *Eur. J. Lipid Sci. Technol.* **2013**, *115* (11), 1224–1238. https://doi.org/10.1002/EJLT.201300049.

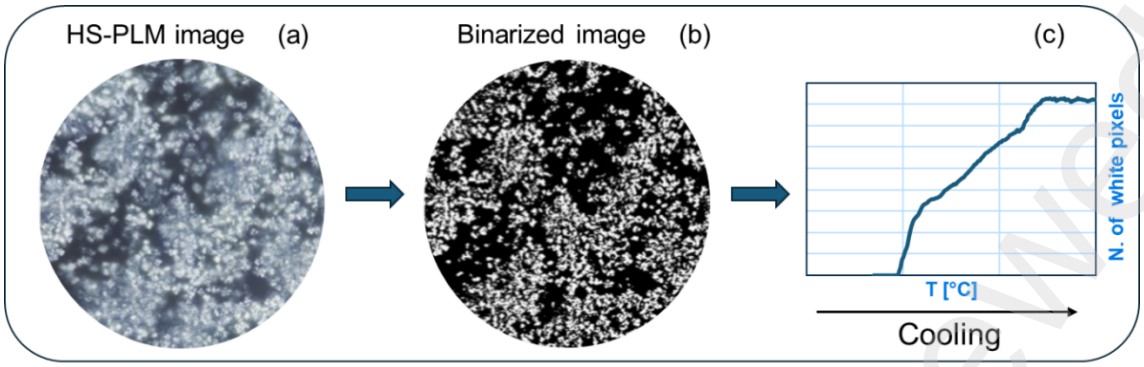

Figure 1. Graphical example of the image processing methodology applied in this work: frames are taken at different temperatures from the video recorded during a crystallization experiment with the at the HS-PLM **(a)**, then the images are processed and binarized in black and with pixels (associated to crystals) **(b)** and from the count of the with pixels in each frame is possible to obtain a plot were the number of pixels (corresponding to the solid crystalline material) are expressed in function of the temperature **(c)**.

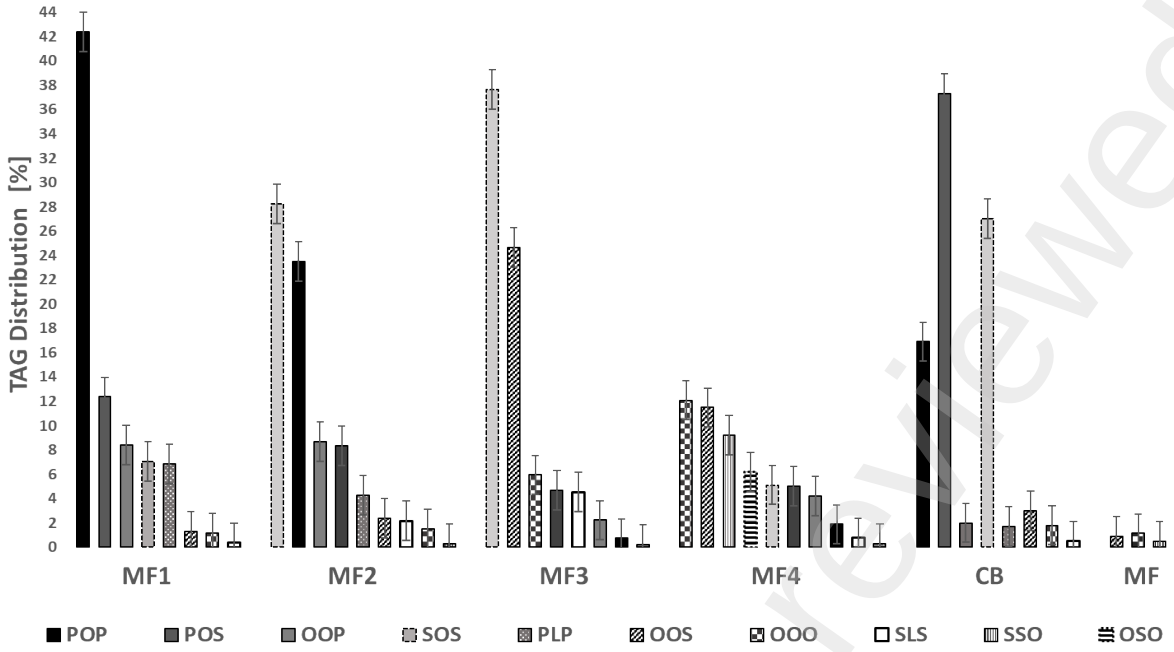

Figure 2. Major TAGs found in compositional characterization of the samples considered in this work.

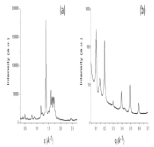

(a)

(b)

Figure 3. CB PXRD diffractogram at 20°C **(a)**; CB SAXS diffractogram at 20°C **(b)**.

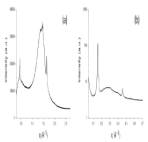

(a)

(b)

Figure 4. MF PXRD diffractogram at 20°C **(a)**; MF SAXS diffractogram at 20°C **(b)**

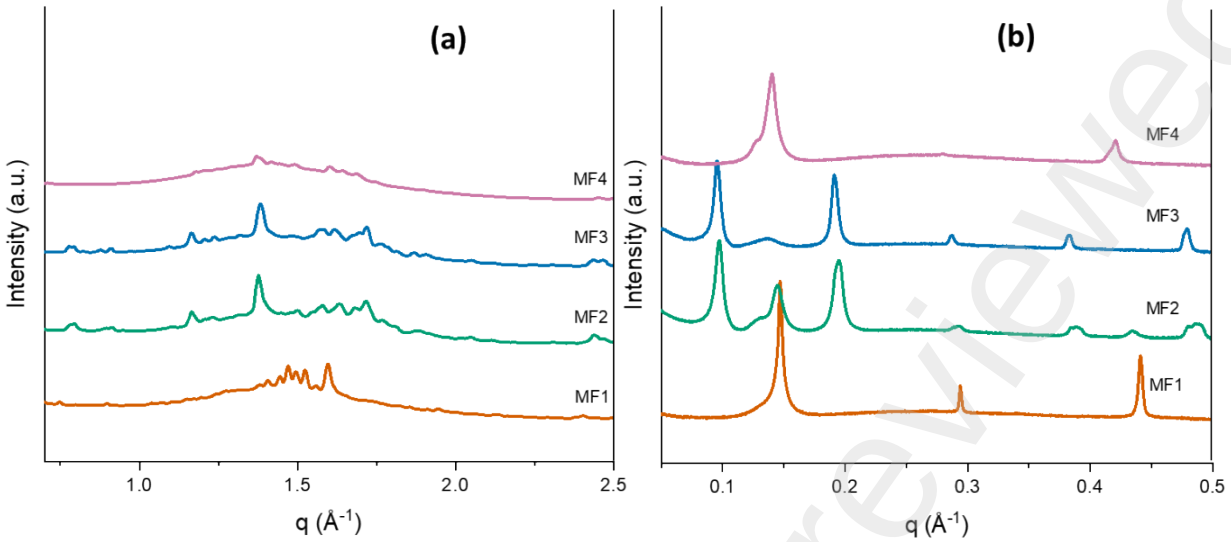

Figure 5. MFn SAXS patterns at 20°C **(a)**; MFn WAXS patterns at 20°C **(b)**

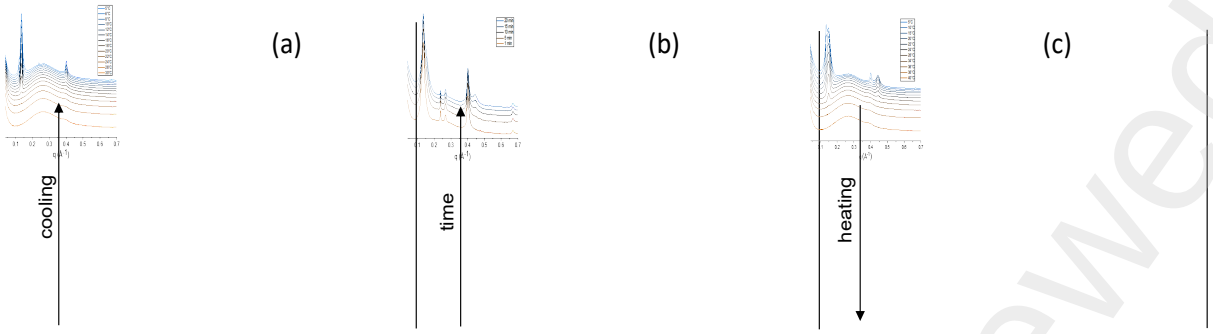

Figure 6. MF1 SAXS temperature profile patterns: cooling **(a)**; holding at 5°C **(b)**; heating **(c)**.

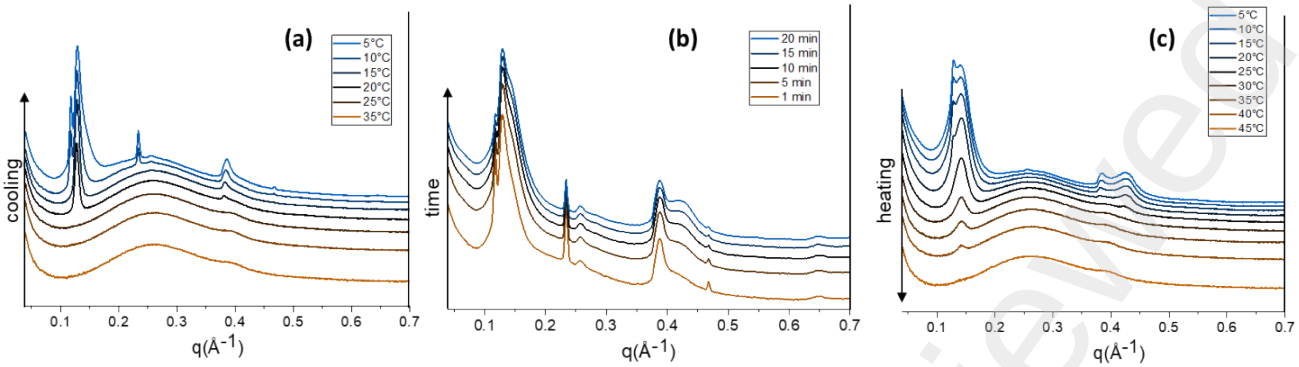

Figure 7. MF2 SAXS temperature profile patterns: cooling profile **(a)**; holding at 5°C **(b)**;heating **(c)**.

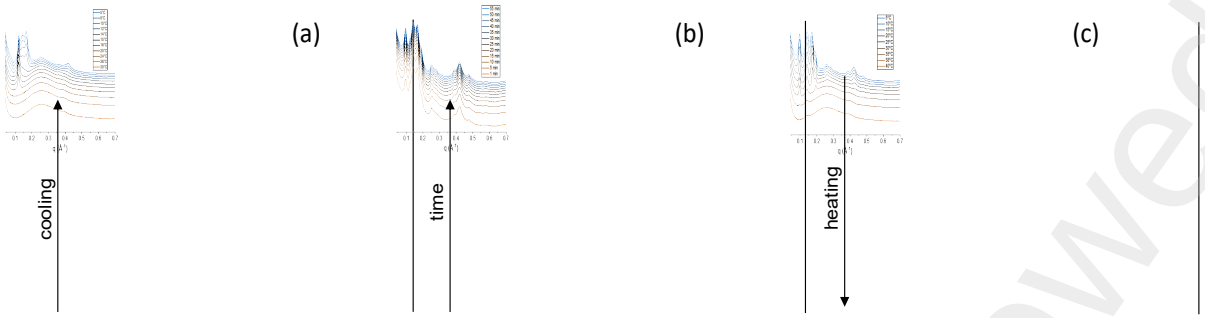

Figure 8. MF3 SAXS temperature profile patterns: cooling **(a)**; holding at 5°C **(b)**; heating **(c)**.

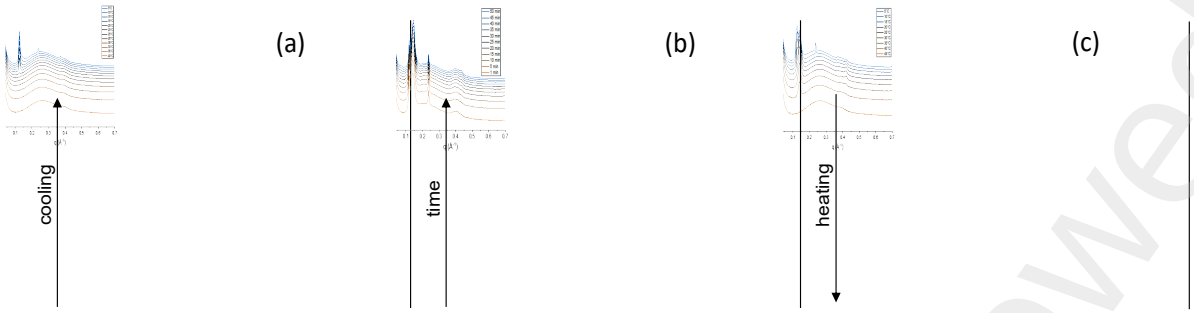

Figure 9. MF4 SAXS temperature profile patterns: cooling **(a)**; holding at 5°C **(b)**; heating **(c)**

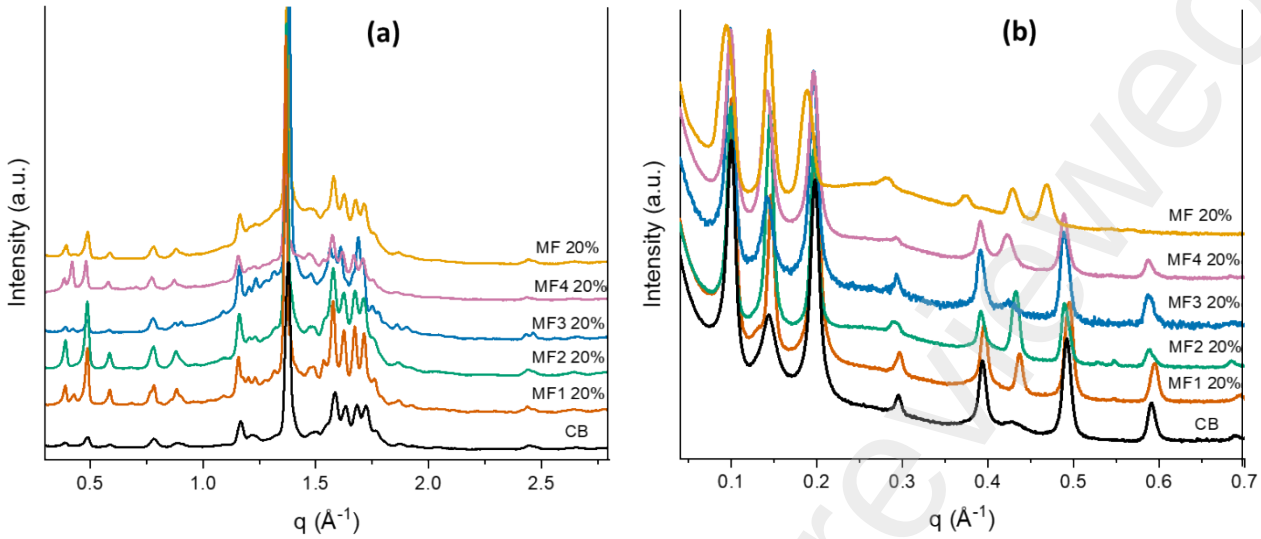

Figure 10. (a) SAXS patterns and **(b)** PXRD diffractogram collected at 20 °C for CB, MFn 20% and MF 20% mixture: CB in black, MF1 20% in brown, MF2 20% in green, MF3 20% in blue, MF4 20% in pink, MF 20% in orange.

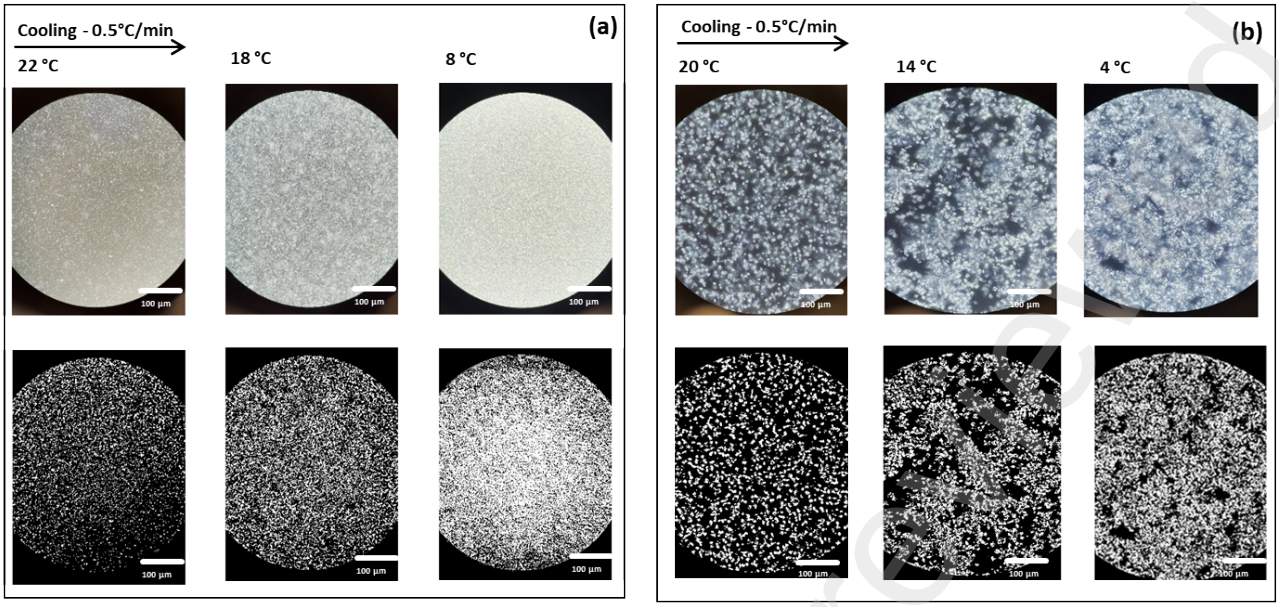

Figure 11. CB **(a)** MF **(b)** Video frames recorded during a crystallization experiment (cooling at -0.5°C/min) with the HS-PLM (Linkam) for CB **(a)** MF **(b)** and their binarized version.

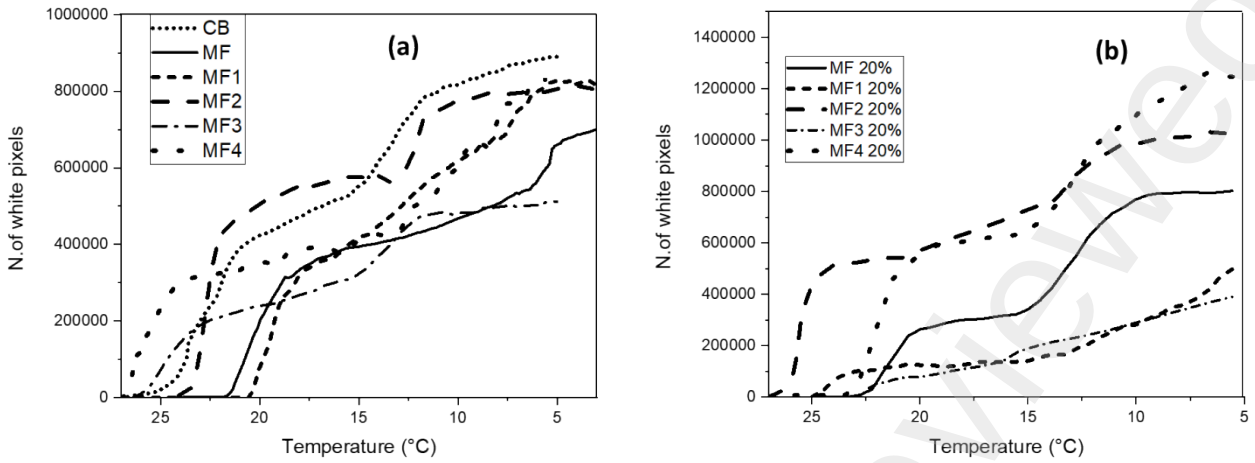

Figure 12. (a) and (b) Plot depicting the results obtained for the HS-PLM experiment at -0.5°C/min. White pixels were counted using a MATLAB script and exported as graph with the number of pixels expressed in function of the Temperature(°C). Pure compounds are shown in figure (a), whereas mixtures at 20% MF or MFn are reported in figure (b)

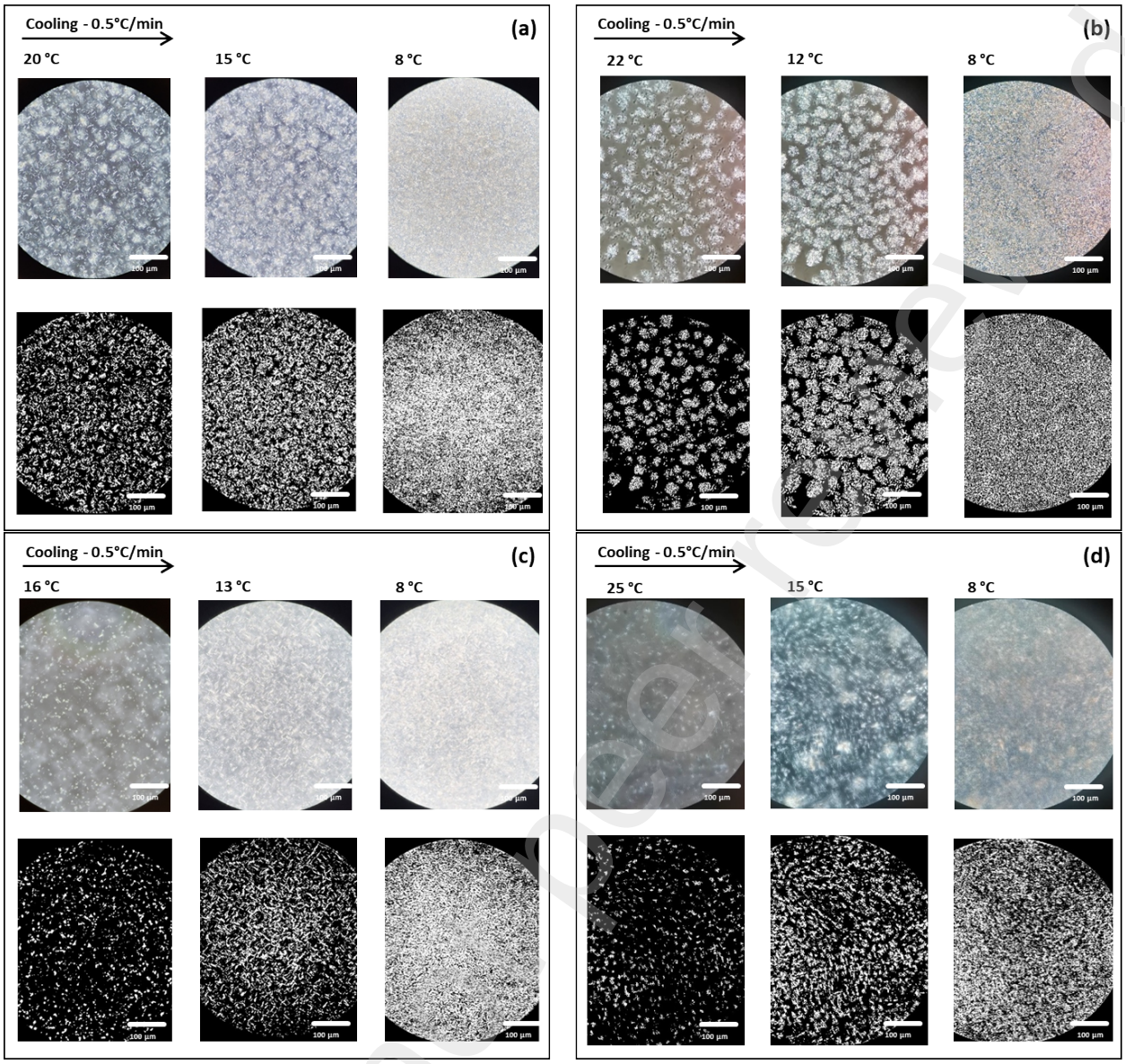

Figure 13. Video frames recorded during a crystallization experiment (cooling at -0.5°C/min) with the HS-PLM (Linkam) for MF1 **(a)**, MF2 **(b)**, MF3 **(c)**, MF4 **(d)**, and their binarized version.

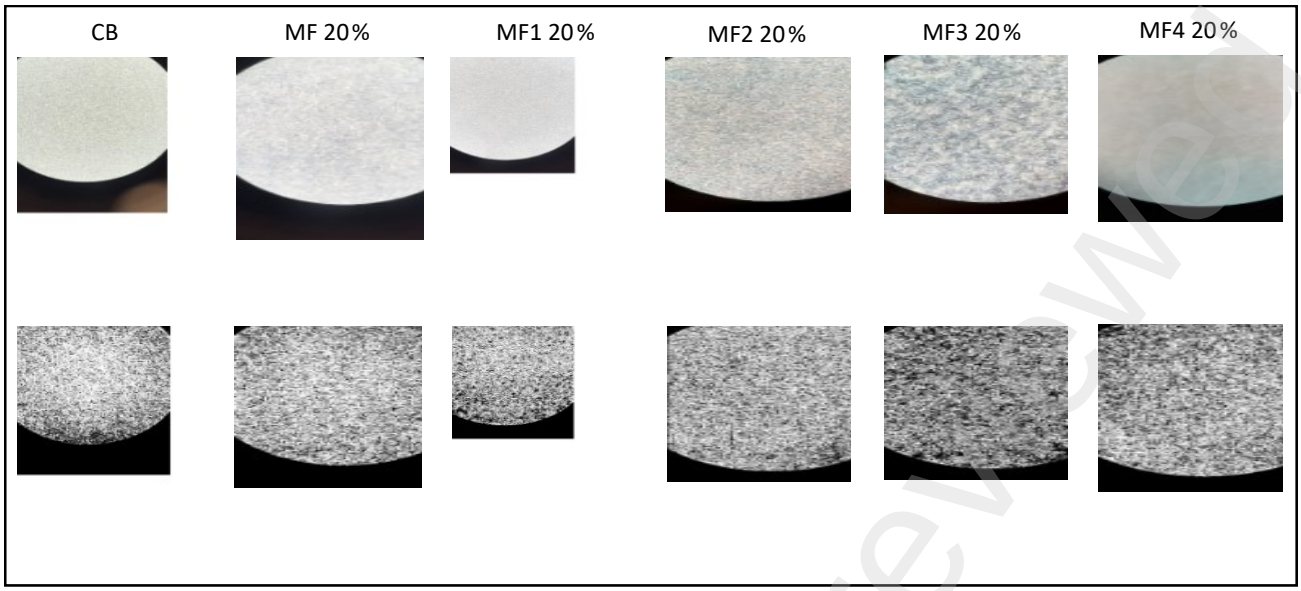

Figure 14. Video frames taken at the end of the crystallization experiment (-0.5°C/min) for CB, MF 20%, and all MF*n* 20% mixture in comparison with each other.

Table 1. Concentration of the most prevalent TAGs in milk fat. [26] Bu stands for butyric acid, P stands for palmitic, M for myristic, S for stearic, O for oleic and Ca for caproic acid.

TAG	Concentration (mol %)
BuPO	4.2
BuPP	3.2
BuMP	3.1
MPO	2.8
POO	2.5
BuPS	2.5
PPO	2.3
PSO	2.2
CaPO	2.0
BuMO	1.8

Table 2. Solid fat contents for all MF*n* (n=1,2,3,4) at different temperatures

Temperature	MF1	MF2	MF3	MF4
20°C	65	42-51	37	25
25°C	39	35-45	36	17
30°C	5	23-30	28	7
35°C	0	0-6	6	3

Table 3. Temperature profiles performed during SAXS measurements.

T (°C) profile	MF*n*/CB/ 20% blends	MF
20°C → 50°C	2°C/min	2°C/min
50°C → 70°C	10°C/min	10°C/min
Holding 70°C	5 min	5 min
70°C → 45°C	-10°C/min	-10°C/min
45°C → 5°C	-0.5°C/min	-0.5°C/min
Holding 5°C	20 min	20 min
5°C → 50°C	0.5°C/min	0.5°C/min
50°C → 5°C	-5°C/min	
Holding 5°C	20 min	

Table 4. TAG composition of MF*n* and CB samples used in this work. P stands for palmitic, S for stearic, O for Oleic acid.

TAG composition (%)	MF1	MF2	MF3	MF4	CB[31]	MF[26]
POP	42.4	23.5	<1	1.9	16.9	3.4
POS	12.4	8.3	4.7	5	37.3	2.3
SOS	7	28.2	37.7	5.1	27	0.6
Tri-saturated	2.7	2.8	3.2	3.9	<1	7.3
Tri-unsaturated	1.7	2.2	7.6	18.8	1.8	1.7
Di-unsaturated	13.5	15.4	33.1	31.1	10	13.3

Table 5. Fatty acid composition of MF*n*, CB and MF analysed samples.

Fatty acids (FA)	MF1	MF2	MF3	MF4	CB	MF
Palmitic (%)	47.6	30	2.8	13.7	25.2	24.4
Oleic (%)	31.5	31.9	41.6	46.1	31.4	19.5
Stearic (%)	11	26.1	37.4	26.7	34.9	4.9
Saturated (%)	58	56	45	38	61	69
Unsaturated (%)	37	39	50	57	34	20
Average FA chain length (number of C)	17.2	17.4	17.9	17.5	17.5	15

Table 6. DSC onset and offset ranges of the thermal events for CB, MF, and MF*n*.

SAMPLE	CB	MF	MF1	MF2	MF3	MF4
Cooling (-2°C/min)	21°C-17°C 15°C-8°C 5°C-0°C	20°C-15°C 16°C-12°C 12°C-0°C	19°C-15°C 10°C-0°C 5°C-(-)2°C	22°C-18°C 15°C-5°C 3°C-2°C	24°C-19°C 15°C-5°C 3°C-2°C	24°C-17°C 15°C-8°C 5°C-2°C
Heating (2°C/min)	10°C-30°C	0°C-11°C 12°C-17°C (exo) 17°C-36°C	5°C-22°C 22°C-34°C	10°C-28°C	-5°C-5°C (exo) 5°C-7°C (exo) 10°C-25°C 25°C-38°C	4°C-6°C 10°C-28°C (exo) 28°C-42°C

Table 7. DSC onset and offset ranges of the thermal events for MF 20% and MF*n* 20% in comaparison with pure CB.

SAMPLE	MF 20%	MF1 20%	MF2 20%	MF3 20%	MF4 20%	CB
Cooling (-2°C/min)	21°C-16°C 15°C-8°C 2°C- (-)2°C	22°C-17°C 16°C-8°C 5°C-0°C	20°C-16°C 16°C-7°C 3°C-(-)2°C	22°C-17°C 17°C-8°C 5°C-0°C	21°C-16°C 15°C-7°C 3°C-(-)1°C	21°C-17°C 15°C-8°C 5°C-0°C
Heating (2°C/min)	5°C-25°C	7°C-30°C	8°C-28°C	5°C-30°C	4°C-28°C	10°C-30°C